WPSA-CPR(17) 17246

N Aiba et al.

Analysis of ELM stability with extended MHD models in existing and future JT-60SA tokamak experiments

Preprint of Paper to be submitted for publication in Proceeding of 44th European Physical Society Conference on Plasma Physics (EPS)

This work has been carried out within the framework of the EUROfusion Consortium and has received funding from the Euratom research and training programme 2014-2018 under grant agreement No 633053. The views and opinions expressed herein do not necessarily reflect those of the European Commission.

Analysis of ELM stability with extended MHD models in existing and future JT-60SA tokamak experiments

N. Aiba 1), S. Pamela 2), M. Honda 3), H. Urano 3), C. Giroud 2), E. Delabie 4), L. Frassinetti 5), I. Lupelli 2), N. Hayashi 3), G. Huijsmans 6,7), the JET Contributors‡ and JT-60SA Research Unit§

1) National Institutes for Quantum and Radiological Science and Technology, Rokkasho, Aomori 039-3212, Japan
2) Culham Centre for Fusion Energy, Abingdon OX143DB, UK
3) National Institutes for Quantum and Radiological Science and Technology, Naka, Ibaraki 319-1112, Japan
4) Oak Ridge National Laboratory, Oak Ridge TN 37831, USA
5) KTH, SE-10041 Stockholm, Sweden
6) CEA, IRFM, F-13108 Saint-Paul-les-Durance, France
7) Eindhoven University of Technology, 5600 MB Eindhoven, The Netherlands

E-mail: aiba.nobuyuki@qst.go.jp

Abstract. The stability to a peeling-ballooning mode (PBM) was investigated numerically with extended MHD simulation codes in JET, JT-60U and the future JT-60SA experiments. The MINERVA-DI code was used for analyzing the linear stability including the rotation and ion diamagnetic drift (ω_{*i}) effects in JET-ILW and JT-60SA plasmas, and the JOREK code was used for simulating nonlinear dynamics with rotation, viscosity and resistivity in JT-60U plasmas. It was validated quantitatively that the ELM trigger condition in JET-ILW plasmas can be explained reasonably by taking into account both the rotation and ω_{*i} effects in the numerical analysis. When the deuterium poloidal rotation is evaluated based on the neoclassical theory, the increase of effective charge of the plasma destabilizes PBM because of accelerating the rotation and decreasing ω_{*i}. The dependence of the amount of ELM energy loss on the rotation direction, which was observed experimentally in JT-60U, was reproduced qualitatively with JOREK. By comparing the ELM affected areas with the linear eigenfunctions, it was confirmed that the difference in the linear stability property due to not the rotation direction but the density profile is thought to be responsible for changing the ELM energy loss just after the ELM crash in JT-60U plasmas rotating in the opposite directions. The predictive study for determining the pedestal profiles in JT-60SA was performed by updating the EPED1 model for including the rotation and ω_{*i} effects in the PBM stability analysis. It was shown that the plasma rotation predicted with the neoclassical toroidal viscosity degrades the pedestal performance about 10% by destabilizing the PBM, but the pressure pedestal height will be high enough to achieve the target parameters required for the ITER-like shape inductive scenario in JT-60SA.

‡ See the author list of Litaudon et al. Overview of the JET results in support to ITER, accepted for publication in Nuclear Fusion.
§ See the author list of JT-60SA Research plan v3.3 at http://www.jt60sa.org/pdfs/JT-60SA_Res_Plan.pdf.

PACS numbers: 52.30.Cv, 52.35.Py, 52.55.Fa, 52.55.Tn, 52.65.Kj

Submitted to: *Plasma Phys. Control. Fusion*

1. Introduction

The high-confinement-mode (H-mode) in tokamak plasmas is usually accompanied by edge localized modes (ELMs), and one of them, called a type-I ELM creates large heat loads on divertor periodically. In future tokamak fusion reactors like ITER and DEMO, the amount of heat loads is thought to be unacceptable because of damaging divertor plates critically. Therefore, it is necessary to develop operation scenario and/or control techniques for avoiding such large ELM heat loads. The important presupposition required to achieve this objective is to predict the plasma conditions triggering the ELM precisely, and fortunately, many past works have shown that ideal MHD stability analysis has evaluated the plasma conditions in experiments successfully [1–3]. These results proved that the type-I ELM is triggered by the ideal MHD mode, called a peeling-ballooning mode (PBM), and the trigger condition is determined by the amount of plasma pressure and current density near edge transport barrier region (pedestal).

However, the type-I ELM was observed experimentally even when the pedestal pressure gradient is much smaller than that predicted numerically in JT-60U and JET with ITER like wall (JET-ILW) [3,4]. The results imply that additional physics effects neglected in the standard ELM stability analysis with the ideal MHD model may be responsible for the ELM stability in these experiments. The main candidates of the effects are the ion diamagnetic drift (ω_i) effect [5], plasma rotation in the toroidal and poloidal directions [3, 5], plasma resistivity [6], and viscosity/diffusivity [7]. A lot of works have been identifying qualitatively the impacts of these effects on both the linear stability and nonlinear dynamics of ELMs with linear and nonlinear MHD simulation codes, such as ELITE [5], MINERVA [8], MINERVA-DI [9], JOREK [10], BOUT++ [7, 11], NIMROD [12, 13], M3D [14, 15], M3D-C1 [6], and so on.

In parallel, some quantitative analyses including a part of these effects have been performed by investigating the stability to PBM with the plasma profiles measured experimentally. For example, the impact of plasma rotation on the ELM stability in JT-60U was identified with MINERVA [3, 8], and this study was revisited by including the ω_{*i} effect simultaneously with the extended linear stability code MINERVA-DI [9] in JT-60U [16] and JET [17]. Furthermore, the impacts of resistivity and viscosity on the ELM in JET-ILW has been investigated with the extended nonlinear stability code JOREK [18]. The results showed that these physics effects play roles determining the ELM trigger conditions in such large tokamak experiments.

In this paper, based on these understandings, we pay attention to the impact of plasma rotation on the stability to PBM when additional physics effects are taken into account simultaneously with MINERVA-DI and JOREK. In section 2, the basic equations used in MINERVA-DI and JOREK are briefly introduced. The results of quantitative analysis of the linear PBM stability in JET-ILW including plasma rotation and ω_{*i} with MINERVA-DI are presented in section 3. After that, we examine the difference of the amount of ELM energy loss in JT-60U plasmas rotating in the opposite directions with JOREK in section 4. In this analysis, finite resistivity is taken into account to simulate magnetic reconnection which is necessary to realize convective heat transport from core to scrape off layer regions. Based on the understandings obtained with the validation studies in the present experiments, we perform the first predictive study for determining the pedestal profiles in JT-60SA [19], and the result is introduced in section 5. Section 6 presents a summary and discussion of this study.

2. Basic equations

In this section, the basic equations of the linear and nonlinear stability codes, MINERVA-DI and JOREK, are introduced briefly; the details are written in [9] and [18], respectively.

The MINERVA-DI code solves the extended Frieman-Rotenberg equation, which is the linearized equation of motion of the diamagnetic MHD model

$$\begin{aligned}\rho_0\frac{\partial^2\boldsymbol{\xi}}{\partial t^2} &+ 2\rho_0(\boldsymbol{V}_{0,MHD}\cdot\nabla)\frac{\partial\boldsymbol{\xi}}{\partial t} + \rho_0(\boldsymbol{V}_{0,*i}\cdot\nabla)\frac{\partial\boldsymbol{\xi}_\perp}{\partial t}\\ &= \boldsymbol{F}_{MHD}+\boldsymbol{F}_{*i}, \qquad (1)\\ \nabla\cdot\boldsymbol{\xi} &= 0, \qquad (2)\end{aligned}$$

with the definition of velocity vectors as

$$\begin{aligned}\boldsymbol{V}_{MHD} &= \boldsymbol{V}_E + V_\parallel\frac{\boldsymbol{B}}{|\boldsymbol{B}|}, \qquad (3)\\ \boldsymbol{V}_E &= \frac{\boldsymbol{E}\times\boldsymbol{B}}{B^2}, \qquad (4)\\ \boldsymbol{V}_{*i} &= \frac{1}{eZ_{eff}NB^2}\boldsymbol{B}\times\nabla p_i. \qquad (5)\end{aligned}$$

Here ρ is the mass density, $\boldsymbol{\xi}$ is the Lagrangian displacement vector, $\boldsymbol{F}_{MHD}$ and $\boldsymbol{F}_{*i}$ are the force operators coming from the ideal MHD and ion diamagnetic correction parts, $\boldsymbol{B}$ is the magnetic field, $\boldsymbol{E}$ is the electric field, e is the quantum of electricity, Z_{eff} is the effective charge, N is the ion number density, p_i is the ion pressure, and the subscript 0 expresses the equilibrium quantity. It should be noted that we introduce the flute approximation $(\boldsymbol{B}_0\cdot\nabla)\boldsymbol{\xi} << 1$ into the diamagnetic correction part for deriving (1). The original diamagnetic MHD model was developed to investigate the impact of the ω_{*i} effect on ideal MHD stability in rotating plasmas, hence, MINERVA-DI realizes to analyze the linear stability to PBM with the rotation and ω_{*i} effects.

The basic equations of the JOREK code are the reduced MHD equations with two equations for the parallel and perpendicular momentum

$$\begin{aligned}\rho\frac{\partial\boldsymbol{V}_E}{\partial t} &+ \rho((\boldsymbol{V}_E+\boldsymbol{V}_{*i})\cdot\nabla)\boldsymbol{V}_E\\ &= \boldsymbol{J}\times\boldsymbol{B}-\nabla_\perp p+\mu\nabla^2(\boldsymbol{V}_E+\boldsymbol{V}_{*i}), \qquad (6)\\ \rho\frac{\partial\boldsymbol{V}_\parallel}{\partial t} &+ \rho(\boldsymbol{V}_\parallel\cdot\nabla)\boldsymbol{V}_\parallel = -\nabla_\parallel p+\mu\nabla^2(\boldsymbol{V}_\parallel-\boldsymbol{V}_{NBI}), \qquad (7)\\ \frac{\partial\psi}{\partial t} &= \eta(J_\phi-J_A)+R[\psi,\Phi]-\frac{\partial\Phi}{\partial\phi}\\ &\quad -\frac{\delta^* R}{\rho}[\psi,p_e]+\frac{\delta^*}{\rho}\frac{\partial p_e}{\partial\phi}, \qquad (8)\\ \frac{\partial\rho}{\partial t} &= -\nabla\cdot(\rho(\boldsymbol{V}_E+\boldsymbol{V}_{*i}))\\ &\quad +\nabla\cdot(D_\perp\nabla_\perp\rho)+S_\rho, \qquad (9)\\ \frac{\partial p}{\partial t} &= -\boldsymbol{V}_E\cdot\nabla p-\Gamma p\nabla\cdot\boldsymbol{V}_E\\ &\quad +\nabla\cdot(\kappa_\perp\nabla_\perp T+\kappa_\parallel\nabla_\parallel T)+S_T, \qquad (10)\end{aligned}$$

with the definition of the operators

$$\nabla_{\parallel} \equiv \frac{\boldsymbol{B}}{|B|}\left(\frac{\boldsymbol{B}}{|B|}\cdot\nabla\right), \tag{11}$$

$$\nabla_{\perp} \equiv \nabla - \nabla_{\parallel}, \tag{12}$$

$$[\alpha,\beta] = R^2\nabla\phi\cdot(\nabla\alpha\times\beta). \tag{13}$$

Here $\boldsymbol{J}$ is the current density, p is the total pressure, μ is the viscosity, ψ is the poloidal magnetic flux, η is the resistivity, J_ϕ is the toroidal current density, R is the major radius, Φ is the electric potential, ϕ is the toroidal angle, $\delta^* \equiv (\Omega_{ci}R_o)$, Ω_{ci} is the ion gyrofrequency, R_o is the reference major radius, p_e is the electron pressure, and $\Gamma = 5/3$ is the specific heat ratio. The NBI momentum, density, temperature, and current sources $\boldsymbol{V}_{NBI}$, S_ρ, S_T and J_A have been introduced. The J_A also includes the time-dependent bootstrap current calculated using Sauter's formula [20, 21]. The perpendicular mass and thermal diffusivities $D_\perp$ and $\kappa_\perp$ used in simulations are ad hoc coefficients with a well at the pedestal region to represent the transport barrier, and the parallel thermal conductivity $\kappa_\parallel$ is expressed to follow the Braginskii one as $\kappa_\parallel = \kappa_{\parallel,o}(T/T_o)^{5/2}$. The basic equations include the effects of rotation, ω_{*i}, resistivity, viscosity, and diffusivities, but in this study, we pay attention to the impact of rotation on the nonlinear ELM dynamics with ad hoc fixed parameters $\eta = 1.0\times10^{-6}[\Omega\cdot m]$, $\mu = 1.0\times10^{-7}[kg(m\cdot s)^{-1}]$, respectively. The $D_\perp$ and $\kappa_\perp$ values are determined to make $D_\perp\nabla\rho$ and $\kappa_\perp\nabla T$ constant in the pedestal region [18], and $D_\perp$ and $\kappa_\perp$ at $\psi = 0.8$ are assumed to be $5.0[m^2s^{-1}]$ and $1.0\times10^{-7}[(ms)^{-1}]$.

3. ELM stability analysis with rotation and the ion diamagnetic drift in JET-ILW

In this section, we investigate the impacts of plasma rotation and ω_{*i} on the stability to MHD modes at edge pedestal in JET with ITER-like wall (JET-ILW). After installing ILW to JET, additional physics effects may be required to explain the ELM trigger condition when the fueling gas rate Γ_D is moderate to high with high heating power (P_h), though the ideal PBM stability can explain the condition when Γ_D is low or P_h is low [4]. As discussed in [16], the rotation can destabilize the modes and help to explain the ELM trigger condition in JET-ILW with high Γ_D and high P_h, though the ELM stability in JET with carbon wall (JET-C) is hardly affected by the rotation. Such a difference comes from the fact that the rotation shear in JET-ILW plasmas was larger than that in JET-C ones, and the shear enhances the dynamic pressure destabilizing intermediate-n MHD modes, where n is the toroidal mode number. In subsection 3.1, we show the result of validation study about the effects of plasma rotation and ω_{*i} on the ELM stability in JET-ILW. After the validation, we confirm the sensitivity of the ELM stability to Z_{eff}.

3.1. Validation study about the impacts of plasma rotation and the ion diamagnetic drift on the ELM stability in JET-ILW

The validation study has been performed by identifying the stability to PBM in 14 JET-ILW shots with different physics models; the summary of the shots is shown in table 1. Here B_{t0} is the magnetic field on axis, I_p is the plasma current, R_0 is the major radius on axis, κ is the ellipticity, δ is the triangularity, β_N is the normalized beta, $\nu_{*e,95}$ is the collisionality at $\psi = 0.95$, respectively. These shots can

Number	B_{t0}[T]	I_p[MA]	R_0[m]	κ	δ	β_N	$\nu_{*e,95}$	Z_{eff}	Γ_D [$\times 10^{21}$el/s]	P_h[MW]	Impurity
89145	1.71	1.38	3.07	1.65	0.260	2.29	0.273	1.65	6.0	13.7	none
90287	1.87	1.37	3.13	1.63	0.263	2.26	0.360	1.86	12.0	16.5	none
90339	1.87	1.37	2.08	1.63	0.262	2.12	0.405	2.45	11.4	16.0	Ne
90337	1.87	1.37	3.10	1.63	0.262	2.11	0.408	2.16	11.7	16.2	Ne
90280	1.87	1.37	3.07	1.61	0.262	2.13	0.458	3.40	11.7	16.2	Ne
82550	2.62	2.48	3.01	1.70	0.370	1.47	0.883	1.26	21.0	16.0	none
87522	2.62	2.46	2.99	1.71	0.373	1.37	1.05	1.49	30.0	29.0	Ne
82554	2.62	2.48	2.98	1.72	0.365	1.34	1.11	1.33	29.0	15.4	N
82551	2.62	2.49	2.99	1.73	0.365	1.48	1.13	1.35	21.7	15.6	N
87520	2.62	2.49	3.02	1.74	0.366	1.36	1.42	1.37	33.0	28.0	Ne
89711	2.62	2.47	3.01	1.70	0.366	1.32	1.47	1.63	40.0	19.0	O
89710	2.62	2.47	3.00	1.70	0.366	1.30	1.53	1.63	40.0	19.0	O
89453	2.62	2.48	2.98	1.75	0.366	1.53	1.57	1.33	17.0	18.0	CD4
89709	2.62	2.47	3.00	1.70	0.366	1.28	1.73	1.50	40.0	19.0	none

Table 1. Summary of the equilibrium parameters in the JET-ILW shots analyzed for the quantitative validation study about the impacts of plasma rotation and ω_{*i} effects on the ELM stability.

be classified into two groups. One is low-$\delta \sim 0.26$, moderate-$\Gamma_D \sim 12.0 \times 10^{21}$[el/s], high-$P_h \sim 16.0$[MW] with $B_{t0} = 1.9$[T] and $I_p = 1.4$[MA], and the other is high-$\delta \sim 0.37$, high-$\Gamma_D > 20.0 \times 10^{21}$[el/s], high-$P_h > 15.0$[MW] with $B_{t0} = 2.6$[T] and $I_p = 2.5$[MA]; only the #89145 plasma, which has the lowest $\nu_{*e,95}$ the analyzed plasmas, was obtained relatively low-$\Gamma_D \sim 6.0 \times 10^{21}$[el/s]. The models are the ideal MHD model without rotation (IDEAL), the diamagnetic MHD model without rotation (DIAwoR), and the diamagnetic one with rotation (DIAwR), respectively. The range of the n number of PBM analyzed numerically is between 1 and 100.

The ELM stability diagram is obtained by analyzing the stability of the equilibria whose pedestal pressure gradient and edge current density are changed by adjusting the height of pressure pedestal and the amount of bootstrap current near the pedestal; the details are written in [16]. The bulk deuterium rotation profiles in both the toroidal and poloidal directions are evaluated with the CHARROT code from the measured profiles of density, temperature, and impurity toroidal rotation (Ω_ϕ) by assuming that the neoclassical theory is applicable [16]. In this study, the Ω_ϕ profile of deuterium is taken into account in both the equilibrium reconstruction and linear stability analysis self-consistently, but the poloidal rotation (Ω_θ) profile is included only in the stability analysis, for simplicity.

As an example, we show the stability diagram of the JET-ILW #90287 plasma in figure 1; the details including the plasma profiles are shown in [22]. By analyzing the stability to PBM with different models on the ($j_{ped,max}$, α_{max}) plane, it was found that the stability boundaries determined with IDEAL is far from the operation point (O.P.), and the ω_{*i} effect moves the boundary away from the O.P. as shown with the DIAwoR result. Here, α_{max} is the maximum normalized pressure gradient defined by $\alpha \equiv -(\mu_0/2\pi^2)(dP_{a0}/d\psi)(dV/d\psi)(V/2\pi^2 R_0)^{0.5}$, $j_{ped,max}$ is the maximum current density in the pedestal region, and width of the error bars on the O.P. are determined

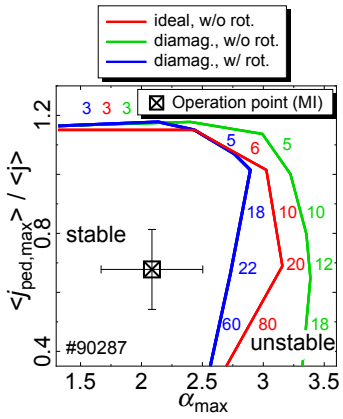

Figure 1. Stability diagram of the JET-ILW #90287 low density plasma on the ($\langle j_{ped,max}\rangle/\langle j\rangle$, α_{max}) plane. The stability boundaries are determined with the different models (IDEAL, DIAwoR and DIAwR). The width of the error bars on the operation point (O.P.) are determined to be $\pm 20\%$ of α_{max} and $\langle j_{ped,max}\rangle$, and the numbers in the figure show the n number of the unstable mode determining the boundary for each model.

to be $\pm 20\%$ of α_{max} and $\langle j_{ped,max}\rangle$, respectively. However, the plasma rotation helps to bring the boundary close to the O.P., and in fact, the DIAwR boundary is the closest one to the O.P. among the results obtained with three models.

Figure 2 (a) shows the $\nu_{*e,95}$ dependence of the distance between the stability boundary and O.P, Δ_α; the Δ_α is defined by $\Delta_\alpha = (\alpha_{max,BND} - \alpha_{max,OP})/\alpha_{max,OP}$. Here $\alpha_{max,BND}$ ($\alpha_{max,OP}$) is the α_{max} value on the stability boundary (O.P.), and $\alpha_{max,BND}$ is the value at the point on the boundary where $\langle j_{ped,max}\rangle$ is equal to that on the O.P.. The error bar of Δ_α is drawn by estimating α_{max} on the boundary where $\langle j_{ped,max}\rangle$ is changed $\pm 20\%$ from that on the O.P.. The Δ_α value determined with the DIAwoR model is larger than 0.4 in 7shots, but those with the IDEAL and DIAwR models are smaller than 0.25 in almost all of the shots analyzed in this study. The result implies that both the IDEAL and DIAwR models can be applicable for the ELM stability analysis in JET-ILW.

However, it should emphasized that the analyses were performed by identifying the stability to PBM whose n number is up to 100, hence, it is necessary for verifying the validity to confirm the n number of the mode determining Δ_α. Figure 2 (b) shows the $\nu_{*e,95}$ dependence of the n number of the mode determining Δ_α. The dependence indicates that the n number of the mode determining the IDEAL Δ_α is 100 in the shots whose $\nu_{*e,95} > 0.88$, and the result implies that the IDEAL stability of such shots is restricted by very high-n modes, including the infinite-n ballooning mode. However, such short wavelength modes usually are not regarded as the trigger of the type-I ELM. In fact, the ω_{*i} effect stabilizes high-n ballooning modes, and the n number of the mode determining the DIAwoR and DIAwR boundaries are always less than 100. The results shown in figure 2 indicate that the ELM trigger condition in JET-ILW can be explained more reasonably by taking into account the rotation and ω_{*i} effects from the viewpoint of small Δ_α and the n number of the mode determining Δ_α.

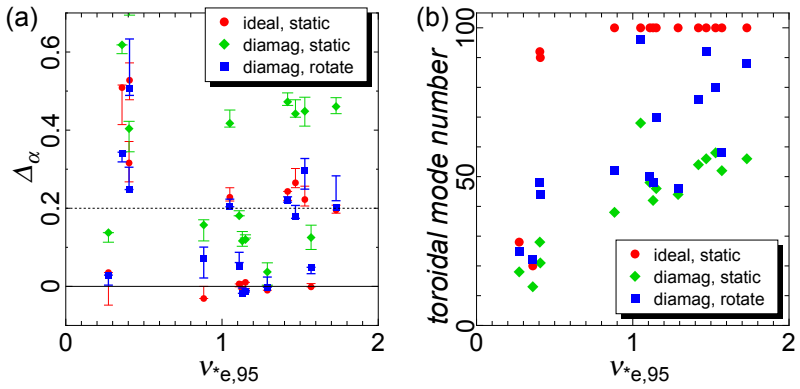

Figure 2. (a) Distance between the operation point and the stability boundary, Δ_α, as a function of the collisionality $\nu_{*e,95}$ at $\psi = 0.95$; the definition of Δ_α is written in the main text. (b) Toroidal mode number of the most unstable mode determining Δ_α for each model as a function of $\nu_{*e,95}$.

3.2. Sensitivity of the ELM stability to effective charge in JET-ILW

When analyzing the ELM stability numerically, the profile of the bulk ion number density, N, is usually determined by

$$N = \frac{Z - Z_{eff}}{Z - 1} n_e, \tag{14}$$

with the assumption that Z_{eff} is constant in the plasma, where Z is the charge of impurity and n_e is the electron number density. The Z_{eff} value in JET-ILW is determined from bremsstrahlung measurements for a line of sight vertical and horizontal independently, hence, the values are sometimes different from each other. For example, in the JET-ILW #89709 plasma, Z_{eff} is estimated as 1.19 when using the horizontal line of sight, which is different from the value estimated with the vertical one as 1.5. Note that Z_{eff} estimated with the vertical line is usually more reliable, hence, the stability analyses in the previous subsection were carried out with the value. In this subsection, the sensitivity of the ELM stability to Z_{eff} is investigated numerically with the JET-ILW #89709 plasma.

When changing Z_{eff}, the number densities of the bulk and impurity ion species become different as (14). Such a difference has impacts on not only p_i but also bootstrap current and rotation profiles evaluated based on the neoclassical theory. Figure 3 shows the profiles of p, $\langle j.B\rangle/\langle B\rangle$, Ω_ϕ, Ω_θ, and ω_{*i} evaluated with the different Z_{eff} values. In the range $1.2 \leq Z_{eff} \leq 1.8$, the profiles of $\langle j.B\rangle/\langle B\rangle$ and Ω_ϕ change little, but the changes in other profiles are visible. It is trivially found that Z_{eff} affects the pressure gradient, and in fact, the α_{max} value on the O.P. changes from 2.20 with $Z_{eff} = 1.5$ to 2.28 and 2.11 with $Z_{eff} = 1.2$ and 1.8, respectively. It should be emphasized that when increasing Z_{eff}, ω_{*i} becomes smaller due to lowering p_i, but Ω_θ increases near pedestal. As discussed in the previous subsection, since plasma rotation can destabilize the ELM but ω_{*i} stabilizes the mode, such a physics trend will make PBM more unstable.

The results of the stability analysis are shown in figure 4; since the n number of the mode determining the IDEAL boundary is 100, only the results with DIAwoR and DIAwR are drawn. When neglecting the rotation effect, only the decrease of ω_{*i}

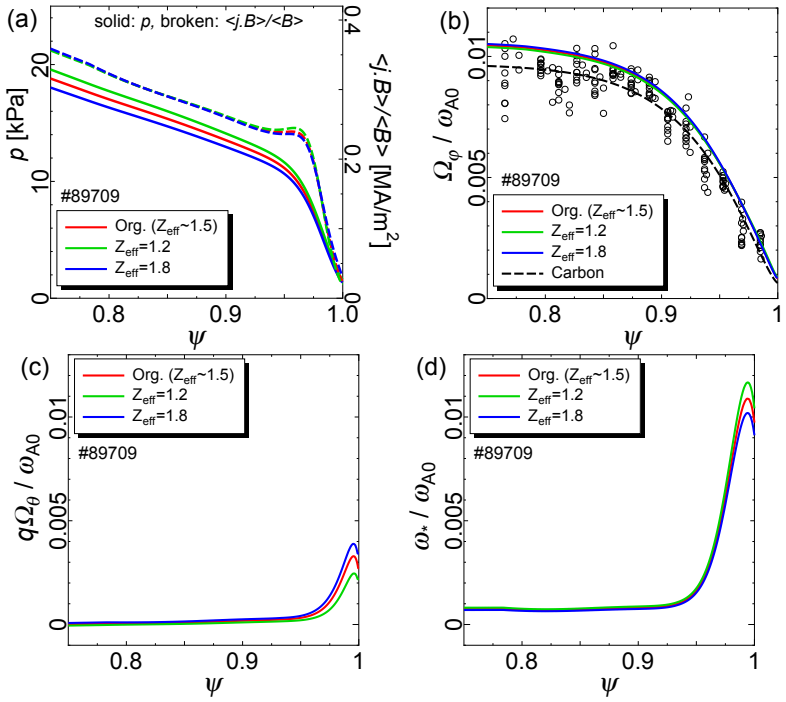

Figure 3. Profiles of the JET-ILW #89709 plasma with different Z_{eff}; (a) p and $\langle \boldsymbol{j} \cdot \boldsymbol{B} \rangle$, (b) Ω_ϕ, (c) Ω_θ, and (d) ω_{*i}.

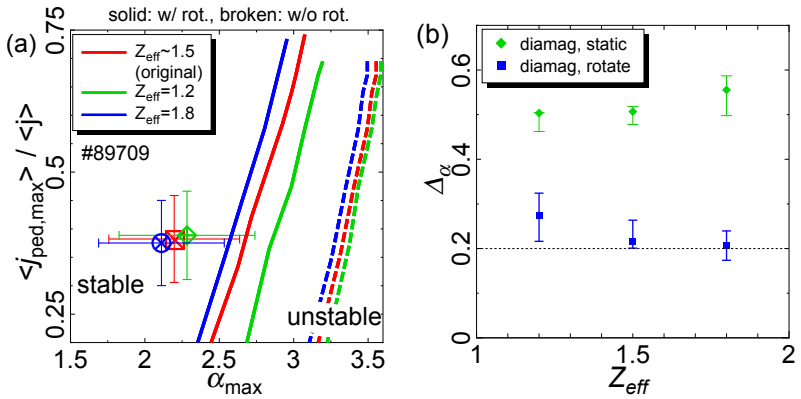

Figure 4. (a) Stability diagrams of the JET-ILW #89709 high density plasma on the $(\langle j_{ped,max} \rangle / \langle j \rangle, \alpha_{max})$ plane determined with the DIAwoR and DIAwR models. The O.Ps. and stability boundaries are determined with the different Z_{eff} values. (b) Δ_α as a function of Z_{eff}.

brings the stability boundary to the lower α_{max} side as Z_{eff} increases as shown in figure 4 (a). As mentioned above, however, α_{max} on the O.P. also decreases as Z_{eff} becomes larger, and as the result, Δ_α tends to become larger as Z_{eff} increases as shown in figure 4 (b). On the other hand, the rotation effect makes the difference in the position of the boundary more visible; namely the rotation can destabilizes the ELM effectively as Z_{eff} increases. In fact, Δ_α decreases from 0.28 with $Z_{eff} = 1.2$ to 0.22 and 0.21 with $Z_{eff} = 1.5$ and 1.8, respectively. Since Z_{eff} does not change the Ω_ϕ profile, it is found that the sensitivity of the ELM stability to Z_{eff} appears due to changing ω_{*i} and Ω_θ. In particular, the difference in Ω_θ, which is estimated based on the neoclassical theory, has large impact on the stability.

4. Nonlinear simulation study of the ELM energy loss in JT-60U rotating plasmas

In this section, we investigate the nonlinear evolution of the type-I ELM in JT-60U plasmas. As discussed in [23], it was confirmed experimentally that the amount of ELM energy loss, ΔW_{ELM}, in the plasma rotating in the co-direction to the plasma current is larger than that rotating in the ctr-rotating one in JT-60U. The rotation direction was changed by adjusting the directions of external momentum input by neutral beam injection (NBI), and hence, in general, not only the rotation but also other plasma profiles are different from each other. In the experiments whose shot numbers are E49228 and E49229, the experimental conditions were set up to minimize such differences, and as the result, the ion temperature (T_i) profiles were almost the same as each other, which were measured with modulation charge exchange recombination spectroscopy (MCXRS). Unfortunately, the electron temperature (T_e) profile could not be measured precisely because of low spatial resolution of Thomson scattering (TS). However, the T_e values near the top of the T_i pedestal were similar to each other, hence, the T_e profile could be regarded as similar to each other by assuming $T_e = 0.6T_i$ in both plasmas. The main difference between these plasmas appears in the electron density (n_e) profile, which was measured with lithium beam probe (LiBP). The n_e pedestal in the co-rotating E49228 plasma was clearly located close to the plasma surface; the details of the profiles are presented in [16, 23]. The linear stability to PBM in these plasmas has been discussed in [3] (with rotation effect) and [16] (with rotation and ω_{*i} effects), and it was confirmed that the rotation has impact on changing the ELM trigger conditions in these plasmas. However, it is not still identified whether the difference in the n_e profiles or the rotation direction is responsible for the amount of ELM energy loss. To resolve the problem, the impacts on nonlinear ELM evolution, including ΔW_{ELM}, are investigated with the JOREK code.

The profiles of the plasmas analyzed in this study are the same as those shown in figure 4 in [16], and their experimental conditions are presented in [23]. In the co-rotating E49228 plasma, The ELM characteristics in the co-rotating E49228 plasma is $\Delta W_{ELM} \simeq 85$[kJ] with the frequency of ELM cycle $f_{ELM} \simeq 37$[Hz], and that in the ctr-rotating E49229 one is $\Delta W_{ELM} \simeq 45$[kJ] with $f_{ELM} \simeq 45$[Hz], respectively. Simulations were run with the full toroidal spectrum from 1 to 15. As discussed with the linear analyses, the plasmas with the original profiles are stable to PBM even when the rotation effect is included, hence, the heights of pressure pedestal are raided about 10% to make PBM marginally unstable in both plasmas; this is thought to be reasonable from the view point of the discrepancy between the O.P. and stability

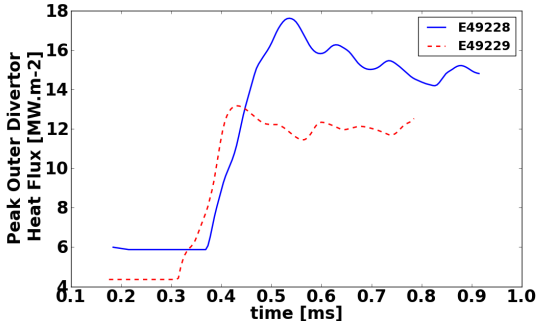

Figure 5. Comparison of peak heat flux to outer divertor in JT-60U E49228 (co-rotating) and E49229 (ctr-rotating) plasmas.

boundary on the ELM stability diagram [3]. Note that the diamagnetic effects are neglected, and only the toroidal rotation is taken into account in this study.

Figure 5 shows the comparison of the heat flux to the divertor in co- (E49228) and ctr- (42999) rotating plasmas. It is clearly observed that the heat load in the co-rotating plasma is larger than that in the ctr-rotating one, and in fact, the ΔW_{ELM} value evaluated between 0.4[ms] and 0.8[ms] in E49228 is 7.3[kJ], which is about 1.5 times larger than that in E49229 (4.6[kJ] between 0.35[ms] and 0.75[ms]). Unfortunately, the majority of ΔW_{ELM} measured experimentally appears within 1.2[ms] just after the ELM crash, and it is obvious that ΔW_{ELM} estimated numerically is much smaller than those in experiment even if the simulation period is extended three times longer. However, even though such a quantitative discrepancy remains between simulation and experiment, the numerical result captures successfully the qualitative trend observed experimentally, hence, it has worth being used for discussing whether n_e or rotation is responsible for changing ΔW_{ELM}.

To answer to the problem, we tried the same simulation by inverting only the rotation direction, and confirmed that ΔW_{ELM} changes little. It should be emphasized that the linear stability to PBM does not change when inverting only the toroidal rotation. This result implies that the rotation direction does not play a major role on changing ΔW_{ELM} between E49228 and E49229 plasmas in JT-60U. Based on the result, we payed attention to the difference in the ELM affected areas observed numerically. Figure 6 (a) shows the change of pressure due to ELM crash, which indicates the ELM affected area. In the colored regions, the amount of lost pressure in the co-rotating plasma is larger than that in the ctr-rotating one; namely, the ELM affected area is wider in the co-rotating plasma. One of the candidates which can explain the trend is the difference in the radial width of the linear eigenfunction of the unstable PBM. Figure 6 (b) shows the comparison of the eigenfunctions in the co- and ctr-rotating plasmas, which are obtained with the ideal MHD code MINERVA. Note that the n number of the most unstable mode is 12 and 15 in each plasma when the n number is truncated from 1 to 15. As is expected, the radial width of the eigenfunction in the co-rotating plasma is wider, and the colored regions, which show where the eigenfunction has larger amplitude, are similar to the ELM affected areas in figure 6 (a). These results indicate that the linear stability property may play a role on determining ΔW_{ELM} emitted in short period just after the ELM crash, and the difference in the property due to not the rotation direction but the density profile

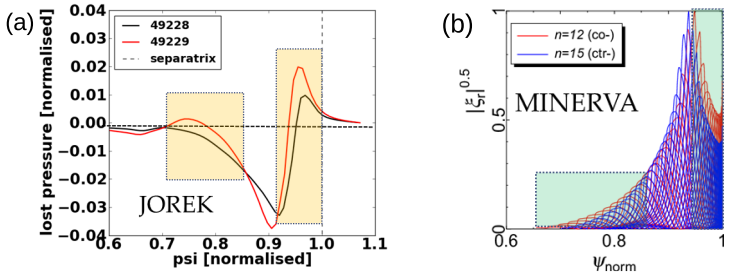

Figure 6. (a) Comparison of the changes of pressure due to ELM crash, which indicates the ELM affected area, in E49228 (co-rotating) and E49229 (ctr-rotating) plasmas. Colored regions show where the lost energy in the co-rotating plasma is larger. (b) Comparison of the linear eigenfuctions of the unstable PBM. Colored regions show where the eigenfunction in the co-rotating plasma has larger amplitude; the square root of the amplitude is plotted to emphasize the difference.

is thought to be responsible for changing ΔW_{ELM} in the analyzed JT-60U plasmas rotating in the opposite directions.

5. Prediction of pedestal conditions with rotation and ω_{*i} effects in JT-60SA

In this section, the ELM stability in the future JT-60SA tokamak experiment is predicted numerically with MINERVA-DI. The pedestal profiles in JT-60SA has been predicted based on the EPED1 model [24] with numerical codes in National Institutes for Quantum and Radiological Science and Technology (QST). In this model, the pedestal width in normalized poloidal flux, Δ, is determined by $\Delta = G(\nu_*, \epsilon, ...)\beta_{\theta,ped}^{0.5}$, where G is a weakly varying parameter, ν_* is the collisionality, ϵ is the inverse aspect ratio, and $\beta_{\theta,ped}$ is the poloidal beta at the top of the pedestal. As discussed in [25], an ensemble average of G, $\langle G \rangle$, obtained with four each typical set of input parameters in DIII-D, JET, AUG and ITER, was obtained as $\langle G \rangle = 0.084 \pm 0.010$. In this study, we used the standard value $\langle G \rangle = 0.076$, which is thought to be determined based on the simplified kinetic ballooning mode (KBM) constraint. Near edge pedestal region, the plasma current is taken to be dominated by the bootstrap current, which is calculated using the matrix inversion method [26]. This bootstrap current and the pressure profiles are determined by assuming the density and temperature profiles with hyperbolic tangent shapes as defined in the EPED1 model.

The pedestal height is usually determined by analyzing the linear stability to PBM with a simple model of diamagnetic stabilization as $\gamma_{MHD} > 0.5\omega_{*pi}$, where γ_{MHD} is the growth rate of the ideal MHD mode in static plasmas, and ω_{*pi} is the half maximum value of the ion diamagnetic frequency in the pedestal. In this study, we have updated the PBM constraint on pedestal height by using the MINERVA-DI code which can include the ω_{*i} effect more self-consistently with rotation effects.

The rotation profile is predicted with the TOPICS code by solving the momentum balance equation with pinch, diffusion, NBI torque and neoclassical toroidal viscosity (NTV) terms [27–29], where the NTV due to the non-axisymmetric perturbed magnetic field caused by toroidal field coils is calculated by coupling TOPICS with the three-dimensional (3D) equilibrium code VMEC [30] and the 3D non-local neoclassical

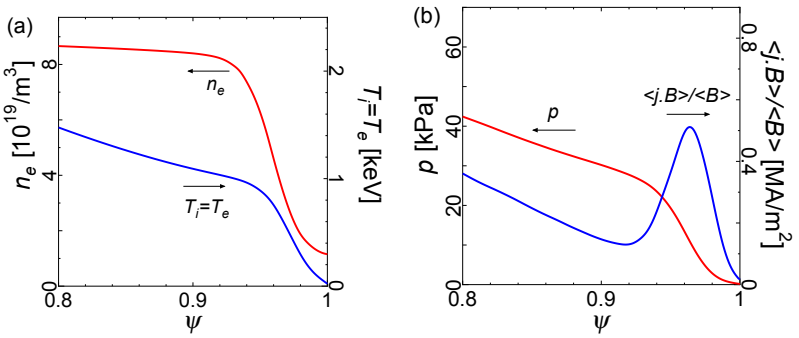

Figure 7. Profiles of the JT-60SA #4-1 plasma; (a) N_e and T_i $(= T_e)$, (b) p and $\langle \boldsymbol{J} \times \boldsymbol{B} \rangle$.

transport simulation code FORTEC-3D [31]. As discussed in [29], the NTV can help to reproduce numerically the toroidal rotation profile observed experimentally, and hence, we investigate the impact of the NTV on the pedestal stability. The boundary condition used for evaluating rotation profiles in this study is assumed as $E_r^{'} = 0$ on the plasma surface, which is determined semi-empirically based on the JT-60U observations [29, 32].

The target plasma analyzed in this study belongs to the JT-60SA plasma operation scenario #4-1, which is called as the ITER-like shape inductive scenario [33–35]. The plasma parameters are $B_{t0} = 2.28$[T], $I_p = 4.6$[MA], $R_0 = 2.94$[m], $a = 1.14$[m], $\kappa_{95} \simeq 1.7$, $\delta_{95} \simeq 0.4$, and $\beta_N \simeq 2.8$, respectively. Since the scenario has a target parameter $n_e/n_{GW} > 0.8$, the height of density pedestal is determined first as $n_{e,ped} = 8.19 \times 10^{19}$[m^{-3}], where n_{GW} is the Greenwald density; in this plasma, $n_{GW} = 1.12 \times 10^{20}$[m^{-3}]. Hence, the height of pressure pedestal is adjusted by changing that of T_i pedestal with the assumption $T_i = T_e$.

First, we have determined the pedestal height with MINEVA-DI under the static plasma assumption; namely, only the ω_{*i} effect is taken into account in the stability analysis. Figure 7 shows the profiles of n_e and $T_i(= T_e)$, and p and $\langle \boldsymbol{J} \cdot \boldsymbol{B} \rangle$ determined with this procedure, respectively; in this case, the height of temperature pedestals is determined to be 1.03[keV].

Based on this reference equilibrium, the impacts of plasma rotation on the ELM stability are investigated. The rotation profiles estimated with the profiles of this equilibrium are shown in figure 8 (a) for the cases with and without the NTV. As shown in this figure, the NTV changes the toroidal rotation profile inside from the vicinity of the inflection point of pressure pedestal, but doesn't affect the poloidal one. With these rotation profiles, the impact of rotation on the stability to PBM is investigated by comparing the stability diagrams obtained with and without the rotation effect; note that the ω_{*i} effect is always taken into account. As shown in figure 8 (b), the operation point exists near the stability boundary determined without rotation. When including the rotation effect, the PBM becomes more unstable, but the rotation profile predicted by neglecting the NTV did not change much the position of the stability boundary; in fact, the difference in the α_{max} values with and without rotation is within 5%. When the rotation is estimated including the NTV, however, the PBM becomes more unstable, and the difference in α_{max} increases to about 10%. Such a difference directly affects the plasma performance, because, as is well-known, the

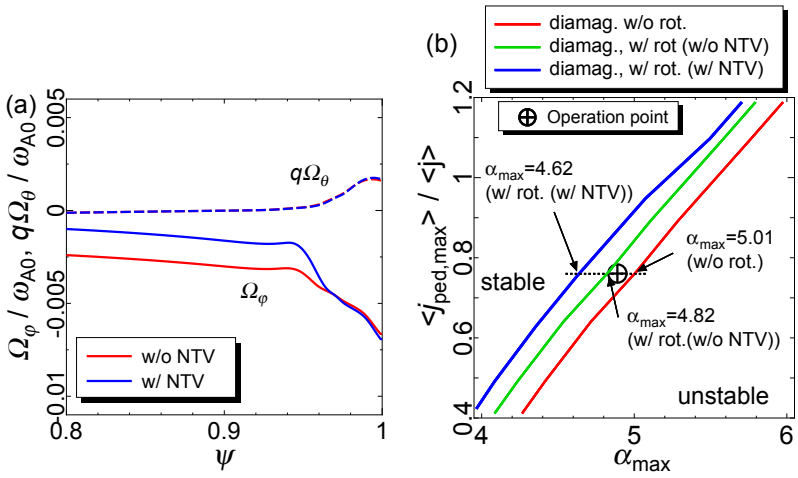

Figure 8. (a) Profiles of Ω_ϕ and Ω_θ calculated with and without the NTV. (b) Stability diagram of the JT-60SA #4-1 plasma on the ($\langle j_{ped,max}\rangle/\langle j\rangle$, α_{max}) plane. The stability boundaries are determined with and without the rotation effect; the ω_{*i} effect is always included. The boundaries determined including the rotation effect are obtained by using the rotation profiles estimated with and without the NTV, respectively.

edge pedestal height mainly determines the boundary conditions for the core plasma. Hence, it is necessary to predict the pedestal conditions by using the latest knowledge and numerical codes, and as one of the examples, the stability analysis including the rotation and ω_{*i} effects will contribute to predict them more precisely. It should be emphasized that the JT-60SA plasma predicted in this study still has large α_{max} value even when the rotation effect is taken into account. We think this is a promising result for achieving the target parameters of the JT-60SA scenario #4-1.

6. Summary

The stability to a peeling-ballooning mode (PBM) in present and future JT-60SA experiments was investigated numerically with two extended MHD simulation codes, MINERVA-DI and JOREK. MINERVA-DI can identify the linear stability to MHD modes with the ion diamagnetic drift (ω_{*i}) effect in rotating tokamak plasmas by solving the extended Frieman-Rotenberg equation corresponding to the diamagnetic MHD model. JOREK solves the reduced MHD equations with two equations for the parallel and perpendicular momentum, and realizes to simulate nonlinear ELM dynamics with rotation, ω_{*i}, resistivity, viscosity, and diffusivities. In this study, the impact of plasma rotation on the stability to PBM was analyzed when the ω_{*i} or the resistivity is taken into account simultaneously.

First, the linear stability to PBM in JET with ITER like wall (JET-ILW) was analyzed including plasma rotation and ω_{*i} effects with MINERVA-DI. After comparing the pedestal pressure gradient which makes the PBM marginally unstable with that observed experimentally in 14 JET-ILW shots, it was found that the ELM trigger condition can be explained more reasonably when both rotation and ω_{*i} effects are taken into account in the numerical stability analyses. The sensitivity of the PBM stability to the effective charge Z_{eff} was also investigated with a JET-ILW plasma,

and the results identified that the stability can be affected by Z_{eff} due to changing ω_{*i}, stabilizing PBM, and poloidal rotation Ω_θ, destabilizing the mode, in the case that Ω_θ is evaluated based on the neoclassical theory.

Next, the amount of ELM energy loss (ΔW_{ELM}) in the JT-60U plasmas rotating in the opposite directions was simulated with finite resistivity and viscosity by using JOREK. In experiments, it was reported that ΔW_{ELM} in the plasma rotating in the co-direction to the plasma current is larger than that rotating in the ctr-direction, and the JOREK simulation realized to reproduce qualitatively the experimental physics trend. By comparing the ELM affected areas determined by the nonlinear simulation with the radial profiles of the eigenfunctions obtained by the ideal linear analysis, it was confirmed that the linear stability property may play a role on determining ΔW_{ELM} emitted in short period just after the ELM crash. The difference in the property due to not the rotation direction but the density profile is thought to be responsible for changing ΔW_{ELM} in the JT-60U plasmas analyzed in this study.

After establishing quantitative understandings about ELM stability property including rotation and ω_{*i} effects, we predicted the pedestal profiles in the future JT-60SA experiment. The procedure for the prediction basically follows the EPED1 model, but the MHD stability, determining the pedestal height, is analyzed with MINERVA-DI to take into account the above effects. In this study, the pedestal of the JT-60SA plasma operation scenario #4-1, the ITER-like shape inductive scenario, was predicted by using the rotation profile estimated with the TOPICS code. It was shown that the plasma rotation estimated including the neoclassical toroidal viscosity effect degrades the pedestal performance about 10% by destabilizing the PBM, but the pressure pedestal height will be high enough to achieve the target parameters required for the scenario.

There are a lot of works left for future. For example, it is necessary to find the key physics causing the large amount of ELM energy loss comparable to the experimental value in JT-60U. One of the candidates is the ELM onset determined by the nonlinear MHD stability with multi harmonics, whose quantitative importance was recently reported in JET simulations with JOREK [18]. Such simulations using JT-60U plasmas are ongoing, and the results will be reported in near future. Further quantitative studies about rotation and ω_{*i} effects on the ELM stability in JET, JT-60U and other present experiments are necessary to complete to validate their importance, and the results will help to predict the ELM stability in future experiments and reactors including JT-60SA, ITER and DEMO. A predictive study for evaluating profiles in the whole region of the core plasma in JT-60SA is also necessary to verify whether the plasma parameters satisfy the target values or not. An integrated simulation with CRONOS is ongoing to predict the profiles of the scenario #4-1 plasma by using the pedestal condition predicted in this study as the boundary condition, and the result will be shown in near future.

Acknowledgments

The authors would like to thank S. Ide, G. Giruzzi for providing an opportunity of the collaborating study between EU and Japan. The authors are grateful to Drs. Y. Kamada, M. Yagi, N. Oyama, C. F. Maggi, E. de la Luna and J. Garcia for beneficial comments and suggestions. Some of the authors (NA and MH) gratefully acknowledges contributions from Drs. S. Satake and Y. Suzuki in NTV calculations. This work was partially supported by JSPS KAKENHI Grant Number 15K06656, and

has been partly carried out within the framework of the EUROfusion Consortium and has received funding from the Euratom research and training programme 2014-2018 under grant agreement No 633053. The views and opinions expressed herein do not necessarily reflect those of the European Commission. The computations were partly carried out using the HELIOS supercomputer system at IFERC-CSC, Aomori, Japan under the Broader Approach collaboration between Euratom and Japan, implemented by Fusion for Energy and Japan. The MARCONI supercomputer at CINECA in Italy was also used for analyzing JET plasmas.

References

[1] Snyder P. B. *et al* 2002 *Phys. Plasmas* **9** 2037.
[2] Saarelma S. *et al* 2005 *Plasma Phys. Control. Fusion* **47** 713.
[3] Aiba N. *et al* 2011 *Nucl. Fusion* **51** 073012.
[4] Maggi C. F. *et al* 2015 *Nucl. Fusion* **55** 113031.
[5] Snyder P. B. *et al* 2007 *Nucl. Fusion* **47** 961.
[6] Ferraro N. M. *et al* 2010 *Phys. Plasmas* **17** 102508.
[7] Xu X. Q. *et al* 2011 *Nucl.Fusion* **51** 103040.
[8] Aiba N. *et al* 2009 *Comput. Phys. Commun.* **180** 1282.
[9] Aiba N. 2016 *Plasma Phys. Control. Fusion* **58** 045020.
[10] Huysmans G. T. A. and Czarny O. 2007 *Nucl. Fusion* **47** 659.
[11] Dudson B. D. *et al* 2009 *Comput. Phys. Commun.* **180** 1467.
[12] Sovinec C. R. *et al* 2004 *J. Comput. Phys.* **195** 355.
[13] Brennan D. P. *et al* 2006 *J. Phys.:: Conf. Ser.* **46** 63.
[14] Park W. *et al* 1999 *Phys. Plasmas* **6** 1796.
[15] Park G. *et al* 2007 *J. Phys.: Conf. Ser.* **78** 012087.
[16] Aiba N. *et al* 2017 *Nucl. Fusion* 022011.
[17] Aiba N. *et al* 2016 *26th IAEA Fusion Energy Conference* TH/8-1.
[18] Pamela S. J. P. *et al* 2017 *Nucl. Fusion* **57** 076006.
[19] Shirai H. *et al* 2017 *Nucl. Fusion* **57** 102002.
[20] Sauter O, *et al* 1999 *Phys. Plasmas* **6** 2834.
[21] Sauter O, *et al* 2002 *Phys. Plasmas* **9** 5140 (erratum).
[22] Aiba N. *et al* 2017 *submitted to Nucl. Fusion*.
[23] Kojima A. *et al* 2009 *Nucl. Fusion* **49** 115008.
[24] Snyder P. B. *et al* 2009 *Nucl. Fusion* **49** 085035.
[25] Snyder P. B. *et al* 2011 *Nucl. Fusion* **51** 103016.
[26] Kikuchi M. and Azumi M. 1995 *Plasma Phys. Control. Fusion* **37** 1215.
[27] Honda M. *et al* 2013 *Nucl. Fusion* **53** 073050.
[28] Honda M. 2014 *Phys. Plasmas* **21** 092508.
[29] Honda M. *et al* 2015 *Nucl. Fusion* **55** 073033.
[30] Hirshman S. P. and van RIJ W. I. 1986 *Comput. Phys. Commun.* **43** 143.
[31] Satake S. *et al* 2008 *Plasma Fusion Res.* **3** S1062.
[32] Kamiya K. *et al* 2014 *Phys. Plasmas* **21** 122517.
[33] Kamada Y. *et al* 2013 *Nucl. Fusion* **53** 104010.
[34] JT-60SA Research Unit 2016 *JT-60SA Research plan version 3.3*.
[35] Garzotti L. *et al* 2017 *accepted to Nucl. Fusion*.